Available online at www.sciencedirect.com

ScienceDirect

Ceramics International 40 (2014) 4345–4350

CERAMICS INTERNATIONAL

www.elsevier.com/locate/ceramint

Synthesis and photoluminescence properties of $La_{1-x}AlO_3:xTb^{3+}$ green phosphors for white LEDs

S.J. Yoon[a], S.J. Dhoble[b], K. Park[a,*]

[a]Faculty of Nanotechnology and Advanced Materials Engineering, Sejong University, Seoul 143-747, Korea
[b]Department of Physics, R.T.M. Nagpur University, Nagpur 440033, India

Received 18 May 2013; received in revised form 25 August 2013; accepted 26 August 2013
Available online 3 September 2013

Abstract

Tb^{3+}-doped $La_{1-x}AlO_3$ phosphor powders are successfully synthesized by the solution combustion method, using citric acid as the combustion fuel. The crystal structure and photoluminescence properties of $La_{1-x}AlO_3:xTb^{3+}$ phosphors are studied, depending on Tb^{3+} content. The strongest emission peak is found at 543 nm, which originates from the $^5D_4 \rightarrow {}^7F_5$ transition of Tb^{3+} ions, indicating green emission. Among the fabricated phosphors, the $La_{0.9}AlO_3:0.1Tb^{3+}$ phosphor emits the strongest green light. The excellent luminescent properties make it a possible candidate for white light-emitting diodes and various photonic applications.

Keywords: A. Mixing; A. Powders: chemical preparation; B. X-ray methods; C. Optical properties

1. Introduction

White light-emitting diodes (LEDs) are considered the next generation light source because of their high brightness, long lifetime, and environment friendliness [1,2]. In 1996, new white LEDs were invented by Nichia Chemical Co. by means of a blue InGaN LED chip coated with yelloow $Y_3Al_5O_{12}$:Ce phosphors [3]. Generally, there are three different approaches which can be used for generating white light based on LEDs: (1) by mixing red (R), green (G), and blue (B) LEDs, (2) by using an ultraviolet (UV) LED and RGB phosphors, and (3) by using a B LED and yellow phosphor. It is considered that a combination of UV LED and RGB phosphors may be the direction of solid-state lighting development due to its high efficiency and high chromatic stability under different driving currents. In the near future, white LEDs will occupy the solid state lighting domain and replace conventional lamps.

Phosphors are usually made from a suitable host material with an added activator. Generally, oxides, nitrides, and sulfides, which have good optical, mechanical, and thermal properties, are used as host materials [4]. Activators such as Eu^{3+}, Tb^{3+}, Dy^{3+}, and Tm^{3+} ions exhibit unique optical behavior when doped into host material. The luminescence of these ions is attributed to the electronic transitions occurring within the partially filled 4f energy shell of the lanthanide series [5]. The remarkable narrow-band emission properties of the rare earth metal ions have been utilized in the development of efficient phosphors [6]. In particular, Tb^{3+} ions are used as activators for efficient blue–green emissions. This originates from the transitions of $^5D_3$ and $^5D_4$ excited states to the ^7F_J ($J=0, 1,\ldots, 6$) ground states of Tb^{3+} ions. When excited by UV radiation, the Tb^{3+} ions ($4f^8$) are raised to the higher $4f^75d^1$ level and feed afterward to the $^5D_3$ or $^5D_4$ excited states [7]. Tb^{3+}-activated phosphors have been widely used in various applications such as three-band fluorescent lamps, projection television tubes, and X-ray intensifying screens [8].

The luminescent properties obtained from rare earth-doped $LaAlO_3$ show a high possibility of $LaAlO_3$ as host materials [9–12]. $LaAlO_3$ is one kind of perovskite-type aluminates and forms a rhombohedral crystal structure [12]. In addition, a solution combustion process is considered to be effective in synthesizing oxide-based nanopowders [13,14]. The basis of the combustion synthesis technique comes from the thermo-chemical concept used in propellant chemistry and explosives [15]. This method exploits an exothermic, chemical reaction

*Corresponding author. Tel.: +82 2 3408 3777; fax: +82 2 3408 4342.
E-mail address: kspark@sejong.ac.kr (K. Park).

0272-8842/$ - see front matter © 2013 Elsevier Ltd and Techna Group S.r.l. All rights reserved.
http://dx.doi.org/10.1016/j.ceramint.2013.08.103

between the desired metal nitrates and a suitable organic fuel. The aim of this study is to synthesize high-quality $La_{1-x}AlO_3$:xTb^{3+} ($0.02 \le x \le 0.2$) phosphor powders by the solution combustion method and to study the photoluminescence (PL) properties of the $La_{1-x}AlO_3$:xTb^{3+} phosphors, depending on the Tb^{3+} content.

2. Experimental

A series of green-emitting $La_{1-x}AlO_3$:xTb^{3+} ($0.02 \le x \le 0.2$) phosphor powders was prepared by the solution combustion method in air. For the solution combustion, metal nitrates are used as the oxidizer, and citric acid is employed as the fuel. The stoichiometric composition of mixtures was calculated based on the total oxidizing and reducing valences of the oxidizer and combustion fuel. The molar ratio of the metal nitrates (oxidizers) to citric acid (fuel) was controlled at 1:1. The starting materials, $La(NO_3)_3 \cdot 6H_2O$ (99.99%, Kanto Chemical Co.), $Al(NO_3)_3 \cdot 9H_2O$ (99.9%, High Purity Chemicals), $Tb(NO_3)_3 \cdot xH_2O$ (99.9%, High Purity Chemicals), and citric acid ($C_3H_4(OH)(COOH)_3$) (99.5%, Duksan Pure Chemicals Co.), were separately dissolved in distilled water. The obtained solutions were mixed and then heated slowly on a hot plate at 120 °C for 7–8 h until water evaporated to form highly viscous gel precursors. The precursors spontaneously ignited to produce voluminous phosphor powders. Finally, the synthesized powders were annealed at 1000 °C for 4 h in air. A schematic diagram showing the experimental procedures for synthesizing the $La_{1-x}AlO_3$:xTb^{3+} ($0.02 \le x \le 0.2$) phosphor powders is shown in Fig. 1.

Several complementary methods were used to characterize the properties of the prepared phosphors. The phase purity and crystallinity of the prepared phosphor powders were characterized with an X-ray diffractometer (XRD; Rigaku RINT2000) using Cu Kα radiation at 40 kV and 100 mA. The morphological characteristics of the powders were investigated with a field emission scanning electron microscope (FE-SEM; Hitachi S4700). The UV PL spectra of the phosphors were obtained with a spectrofluorometer (QM-4/2005SE, PTI, USA) equipped with a 75 W Xenon lamp. All the measurements were conducted at room temperature.

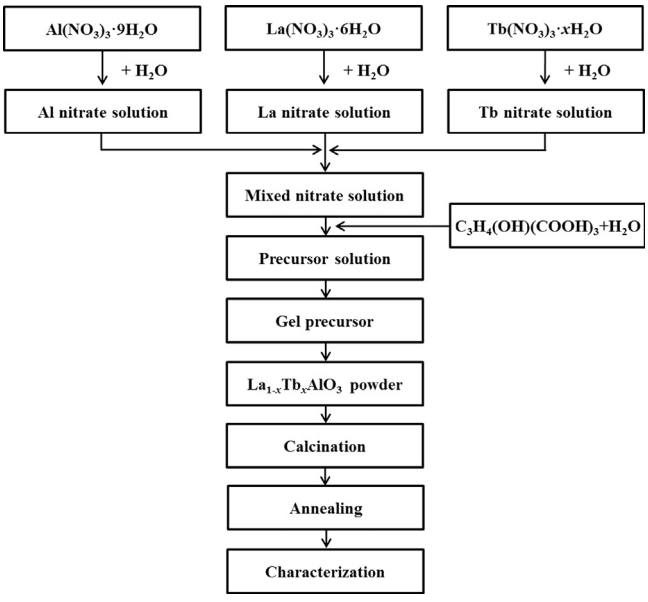

Fig. 1. A schematic diagram showing the experimental procedures for synthesizing the $La_{1-x}AlO_3$:xTb^{3+} ($0.02 \le x \le 0.2$) phosphor powders.

3. Results and discussion

The XRD patterns of $La_{1-x}AlO_3$:xTb^{3+} ($0.02 \le x \le 0.2$) phosphor powders are shown in Fig. 2. These patterns reveal that the crystal structure of the $La_{1-x}AlO_3$:xTb^{3+} powders is rhombohedral [11,12,16]. The reflections caused by any impurities are not detected. This is due to the extremely homogeneous mixing of the constituent materials on an atomic scale and the exothermic and self-sustaining reaction. The crystallite size of the $La_{1-x}AlO_3$:xTb^{3+} powders can be calculated from the broadening of diffraction peaks by the following Scherrer's formula [17]:

$$D = (0.9\lambda/\beta \cos \theta) \quad (1)$$

where λ is the wavelength of radiation, θ is the angle of the diffraction peak, and β is the full width at half maximum of the diffraction peak (in radian). The calculated crystallite sizes decrease with an increase in Tb^{3+} content, ranging from 30.1 to 38.0 nm (Fig. 3).

FE-SEM images of the annealed $La_{1-x}AlO_3$:xTb^{3+} powders with x=0.02 and 0.1 are shown in Fig. 4(a) and (b), respectively. The morphology of the powders with other Tb^{3+} contents is quite similar to that of these figures. All the fabricated $La_{1-x}AlO_3$:xTb^{3+} ($0.02 \le x \le 0.2$) powders show nanocrystalline nature. The combustion processing used here for synthesizing nano-sized $La_{1-x}AlO_3$:xTb^{3+} powders is fairly simple, fast, and cost-effective compared to the conventional solid-state reaction method. In addition, the method does not involve intermediate decomposition or calcination steps. In this respect, a solution combustion process is favorable for synthesizing pure and nanocrystalline $La_{1-x}AlO_3$:xTb^{3+}

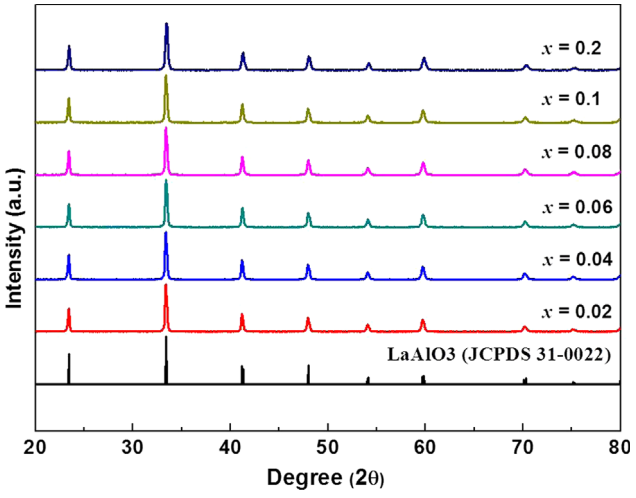

Fig. 2. XRD patterns of the $La_{1-x}AlO_3$:xTb^{3+} ($0.02 \le x \le 0.2$) phosphor powders.

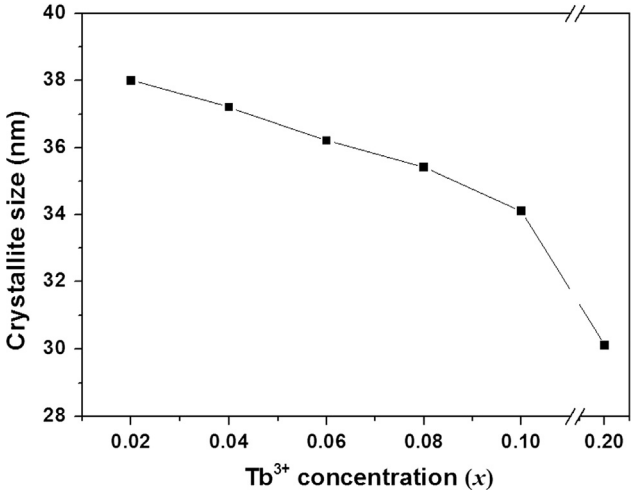

Fig. 3. Crystallite sizes of the $La_{1-x}AlO_3:xTb^{3+}$ ($0.02 \le x \le 0.2$) phosphor powders.

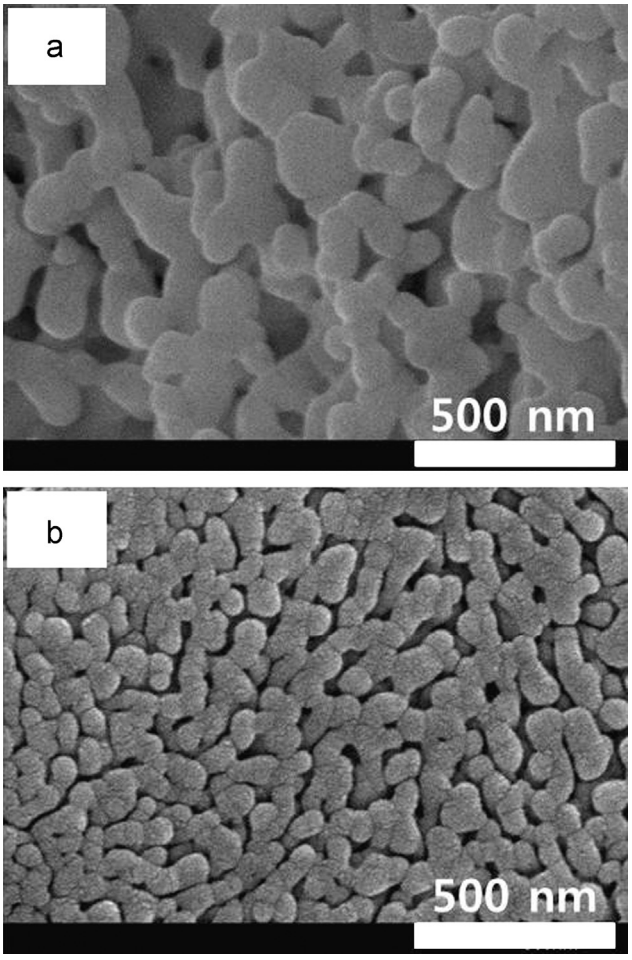

Fig. 4. FE-SEM images of the annealed $La_{1-x}AlO_3:xTb^{3+}$ phosphor powders with x=(a) 0.02 and (b) 0.1.

oxides, along with improved powder characteristics, thus engendering great interest in its optical properties [18,19]. The powder sizes decreases with an increase in Tb^{3+} content. This is because the dopant Tb^{3+} lowers the potential barrier for the formation of nuclei and inhibits the growth rate of nuclei [20].

The excitation spectra of the $La_{1-x}AlO_3:xTb^{3+}$ ($0.02 \le x \le 0.2$) phosphors, monitored at 543 nm, are shown in Fig. 5. It can be seen that the excitation spectra consist of two broad bands (243 and 256 nm; Fig. 5(a)) and several sharp peaks (280–393 nm; Fig. 5(b)). This clearly indicates that the phosphors can be effectively excited by UV. The excitation peaks centered at 243 and 256 nm may be attributed to the $LaAlO_3$ host absorption and terbium–oxygen charge-transfer, respectively [11]. In addition, the excitation peaks at 280–393 nm may be caused by the $4f \rightarrow 4f$ transitions of Tb^{3+} ions [21]. The excitation intensities increase with an addition of Tb^{3+} content and reach the maximum when the content of Tb^{3+} ions is 0.1.

The emission spectra of the $La_{1-x}AlO_3:xTb^{3+}$ ($0.02 \le x \le 0.2$) phosphors, recorded under the 256 nm excitation, are shown in Fig. 6. The emission spectra exhibit two major emission peaks at around 543 and 582 nm, which are attributed to the $^5D_4 \rightarrow {}^7F_5$ and $^5D_4 \rightarrow {}^7F_4$ transitions of Tb^{3+} ions, respectively [22]. The strongest emission peak is located at 543 nm, which is responsible for green emission. The emission peak caused by the $^5D_4 \rightarrow {}^7F_5$ transition is split into two peaks (543 and 550 nm), and that caused by the $^5D_4 \rightarrow {}^7F_4$ transition

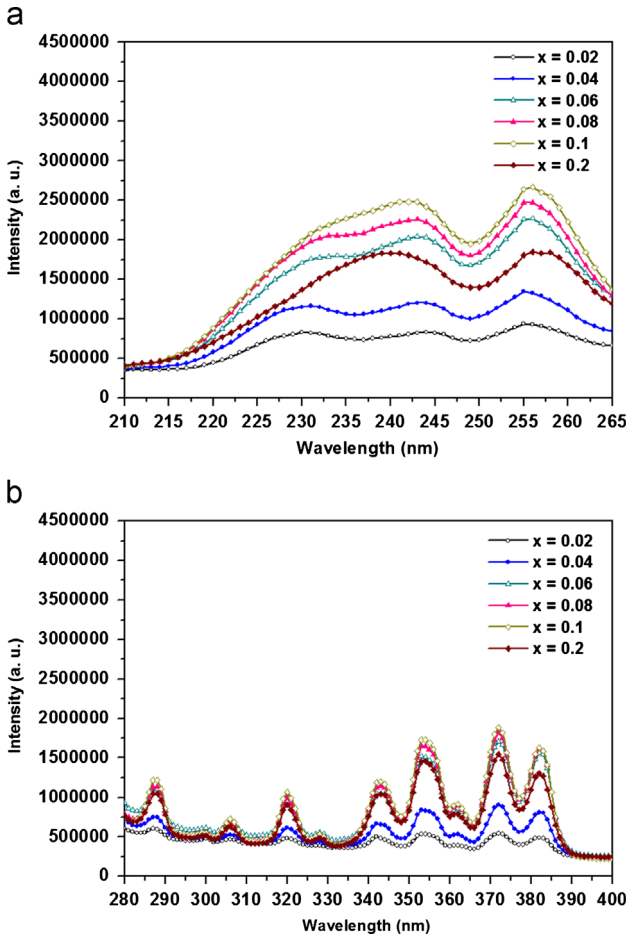

Fig. 5. Excitation spectra of the $La_{1-x}AlO_3:xTb^{3+}$ ($0.02 \le x \le 0.2$) phosphors: (a) 210–265 nm and (b) 280–400 nm.

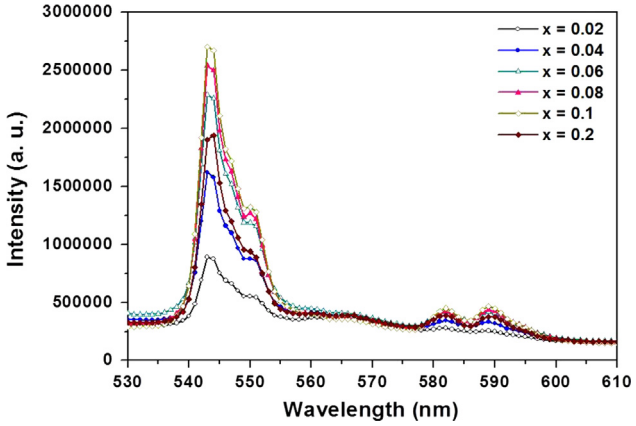

Fig. 6. Emission spectra of the $La_{1-x}AlO_3:xTb^{3+}$ ($0.02 \le x \le 0.2$) phosphors.

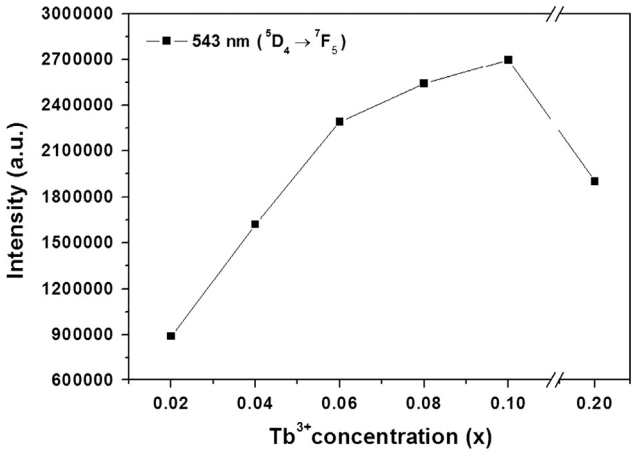

Fig. 7. Emission intensities centered at 543 nm for the $La_{1-x}AlO_3:xTb^{3+}$ ($0.02 \le x \le 0.2$) phosphors.

is split into two peaks (582 and 589 nm). These splits are related to the crystal field effect [23]. A similar result was reported in the $LiBaBO_3:Tb^{3+}$ phosphors studied by Li et al. [23]. They reported that under 365 nm excitation, the emission spectrum of $LiBaBO_3:Tb^{3+}$ phosphors showed four major emission bands at 488, 544, 593, and 616 nm, which were attributed to the $^5D_4 \rightarrow {}^7F_6$, $^5D_4 \rightarrow {}^7F_5$, $^5D_4 \rightarrow {}^7F_4$, and $^5D_4 \rightarrow {}^7F_3$ transitions of Tb^{3+} ions, respectively. These emission peaks are split as follows: the energy level transition $^5D_4 \rightarrow {}^7F_6$ is split into 488 and 493 nm peaks; $^5D_4 \rightarrow {}^7F_5$ is split into 544 and 549 nm peaks; $^5D_4 \rightarrow {}^7F_4$ is split into 583, 590, 593, and 596 nm peaks; and $^5D_4 \rightarrow {}^7F_3$ is split into 616, 620, and 623 nm peaks.

The $La_{1-x}AlO_3:xTb^{3+}$ phosphors with different Tb^{3+} contents display quite similar emission spectra except for emission intensity. It is clear that the emission intensity depends strongly on the content of Tb^{3+} ions. The emission intensities centered at 543 nm as a function of Tb^{3+} content are shown in Fig. 7. The emission intensity increases with Tb^{3+} content up to $x=0.1$ due to the larger number of luminescent centers and then decreases with the further increased Tb^{3+} content, owing to the energy transfer between the neighboring Tb^{3+} ions, i.e., quenching of the emission of Tb^{3+} [24]. The energy transfer occurs from one Tb^{3+} activator to another until an energy sink in the lattice is reached [25]. Non-radiative energy transfer plays an important role for technological design considerations and for the basic understanding of the physical excitation processes involved [26]. Quantitative theories of non-radiative energy transfer, based on resonance transfer by electric multipole–multipole interaction or exchange interaction, were proposed [27]. Dexter [28] included transfer by means of forbidden transitions to extend the resonance theory of Förster, which involves only allowed transitions. Dexter and Schulman [29] presented a theory for concentration quenching in solid systems, based on the migration of excitation energy from one activator center to another and eventually to an imperfection which may act as an energy sink. They discussed the dependence of the fluorescence yield on concentration and typical activator concentrations at which appreciable quenching may be expected to occur. Berdowski and Blasse [30] claimed that the interaction between the Eu^{3+} ions in two-dimensional compounds is due to a super-exchange interaction and not a multipole–multipole interaction. The super-exchange interaction occurs by the spin exchange via the electron orbital of the oxygen atom [31]. When the nature of the interaction is the super-exchange, the interaction between the second nearest neighbor Eu^{3+} ions becomes important. The number of Eu^{3+} ions interacting with the other ions is larger than the number of nearest neighbors for the square lattice. It is thus necessary to evaluate the critical distance for energy transfer, the distance among activator ions at the regime of concentration quenching.

The critical transfer distance (R_0) from the concentration quenching can be calculated using the following formula [32]:

$$R_0 = 2\left(\frac{3V}{4\pi x_c N}\right)^{1/3} \quad (2)$$

where R_0 is the critical concentration at which the quenching occurs, N is the number of La^{3+} ions in the $LaAlO_3$ unit cell, and V is the volume of the unit cell. By taking the experimental and analytic values, the critical transfer distance of Tb^{3+} in the $La_{1-x}AlO_3:xTb^{3+}$ phosphors is calculated to be 18.4 Å. The values of x_c, N, and V used here are 0.1, 1, and 326.7 Å, respectively. Previous researchers reported the calculated critical concentration (R_0) of oxidic phosphors, i.e., 18, 16, 15, 22, 18, 18, 17.32, 27.15, and 16.7 Å for $YPO_4:Ce^{3+}$, $LaPO_4:Ce^{3+}$, $Y_3Al_5O_{12}:Ce^{3+}$, $BaBPO_4:Eu^{2+}$, $SrO \cdot Al_2O_3:Eu^{2+}$, $Ca_2MgSi_2O_7:Eu^{2+}$, $Ba_2Mg(BO_3)_2:Eu^{2+}$, $Ba_{1.3}Ca_{0.7}SiO_4:Ce^{3+}$, and $NaCa_4(BO_3)_3:Eu^{3+}$, respectively [25,27,33–36]. Non-radiative energy transfer from one activator to another may occur by exchange interaction, radiation reabsorption, or multiple–multiple interaction [34,35]. According to a previous study [34], multipole–multipole interaction currently occurs when the distance between two ions is about 20 Å. The critical transfer distance (18.4 Å) calculated here means that the multipole–multipole interaction may occur in the Tb^{3+} of $La_{1-x}AlO_3:xTb^{3+}$ phosphor.

Fig. 8 depicts an energy level showing the transition of Tb^{3+} ions and the luminescence mechanism. All the emission

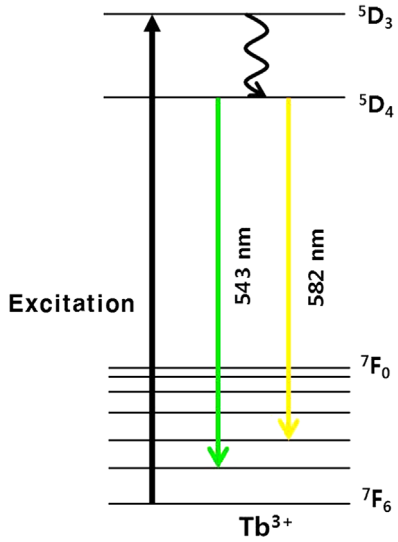

Fig. 8. A schematic diagram showing the transition of Tb^{3+} ions and the luminescence mechanism.

peaks peaking at 543 and 582 nm are caused by the transitions from the energy level $^5D_4$ to ^7F_J ($J=5$ and 4) of Tb^{3+} ions. According to this luminescence mechanism, Tb^{3+} ions are first excited from the ground state to the excited state $^5D_2$, drop down non-radiatively to the excited level $^5D_4$, and finally fall down radiatively to the energy levels of ^7F_J ($J=5$ and 4) [37]. The $La_{1-x}AlO_3{:}xTb^{3+}$ phosphors studied here exhibit enhanced PL characteristics owing to the high purity and nanocrystalline nature of the powders. In this respect, the solution combustion method is favorable for preparing high-quality green $La_{1-x}AlO_3{:}xTb^{3+}$ phosphors. It is considered that the $La_{1-x}AlO_3{:}xTb^{3+}$ phosphor can be used as a green emitting phosphor for white LEDs and various photonic applications.

4. Conclusions

We prepared nano-sized $La_{1-x}AlO_3{:}xTb^{3+}$ ($0.02 \le x \le 0.2$) phosphor powders by the solution combustion method, using citric acid ($C_3H_4(OH)(COOH)_3$) as the combustion fuel. The solution combustion process provided a very attractive route for producing high-quality $La_{1-x}AlO_3{:}xTb^{3+}$ phosphor powders. The annealed $La_{1-x}AlO_3{:}xTb^{3+}$ phosphor powders crystallized in rhombohedral structure. In the excitation spectra, two broad bands (243 and 256 nm) and several sharp peaks (280–393 nm) were observed. By increasing Tb^{3+} content, the excitation intensities were increased and reached the maximum at $x=0.1$. The emission spectra exhibited two major emission peaks at 543 and 582 nm, which were attributed to the $^5D_4 \rightarrow {}^7F_5$ and $^5D_4 \rightarrow {}^7F_4$ transitions of Tb^{3+} ions, respectively. The emission intensities of $La_{1-x}AlO_3{:}xTb^{3+}$ phosphors increased with increasing Tb^{3+} content, and the maximum intensity was obtained at $x=0.1$. The critical transfer distance of Tb^{3+} in the $La_{1-x}AlO_3{:}xTb^{3+}$ phosphors was calculated to be 18.4 Å. From the excitation and emission spectra, the $La_{1-x}AlO_3{:}xTb^{3+}$ phosphors can be effectively excited by UV light (256 nm) and exhibited a satisfactory green emission (543 nm), thus fitting in with the widely applied UV LED chip.

References

[1] W. Lv, N. Guo, Y. Jia, Q. Zhao, H. You, A potential single-phased emission-tunable silicate phosphor $Ca_3Si_2O_7{:}Ce^{3+}$, Eu^{2+} excited by ultraviolet light for white light emitting diodes, Optical Materials 35 (2013) 1013–1018.
[2] B. Han, J. Zhang, Q. Cui, Y. Liu, A potential reddish or an green emitting phosphor $Ca_2BO_3Cl{:}Eu^{3+}$ for white light-emitting diodes, Physica B 407 (2012) 3484–3486.
[3] S. Ye, F. Xiao, Y.X. Pan, Y.Y. Ma, Q.Y. Zhang, Phosphors in phosphor-converted white light-emitting diodes: recent advances in materials techniques and properties, Materials Science and Engineering R 71 (2010) 1–34.
[4] H.A.A.S. Ahmed, O.M. Ntwaeaborwa, R.E. Kroon, High efficiency energy transfer in Ce, Tb co-doped silica prepared by sol–gel method, Journal of Luminescence 135 (2013) 15–19.
[5] S.C. Gedam, S.J. Dhoble, S.V. Moharil, 5d–4f transition in halosulphate phosphors, Journal of Luminescence 126 (2007) 121–129.
[6] V. Natarajan, A.R. Dhobale, C.H. Lu, Preparation and characterization of tunable $YVO_4{:}Bi^{3+}$, Sm^{3+} phosphors, Journal of Luminescence 129 (2009) 290–293.
[7] J.-Y. Park, H.-C. Jung, G.S.-R. Raju, B.-K. Moon, J.-H. Jeong, J.-H. Kim, Solvothermal synthesis and luminescence properties of Tb^{3+}-doped gadolinium aluminum garnet, Journal of Luminescence 130 (2010) 478–482.
[8] S.P. Khatkar, S.D. Han, V.B. Taxak, G. Sharma, D. Kumar, The influence of sintering temperature on particle size/shape and photoluminescence characteristics of $CaIn_2O_4{:}x$Tb synthesized by combustion process, Optical Materials 29 (2007) 1362–1366.
[9] X. Dong, X. Cui, Z. Fu, S. Zhou, S. Zhang, Z. Dai, Study on preparation and luminescent properties of Eu^{3+}-doped $LaAlO_3$ and $GdAlO_3$, Materials Research Bulletin 47 (2012) 212–216.
[10] P.J. Dereń, M.A. Weglarowicz, P. Mazur, W. Strek, Spectroscopic properties of $LaAlO_3$ nanocrystals doped with Tb^{3+} ions, Journal of Luminescence 122–123 (2007) 780–783.
[11] B. Chen, J. Yu, X. Liang, $LaAlO_3$ hollow spheres: synthesis and luminescence properties, Langmuir 27 (2011) 11654–11659.
[12] E. Antic-Fidancev, P.J. Deren, J.C. Krupa, Energy levels and crystal field calculations of Er^{3+} in $LaAlO_3$, Journal of Alloys and Compounds 380 (2004) 376–379.
[13] K. Park, K.Y. Kim, M.H. Heo, VUV photoluminescence of $(Y_{0.5}Gd_{0.5})_{0.94}VO_4{:}Eu^{3+}$ red-emitting phosphors prepared by solution combustion method, Materials Research Bulletin 47 (2012) 4151–4155.
[14] K. Park, M.H. Heo, K.Y. Kim, S.J. Dhoble, Y. Kim, J.Y. Kim, Photoluminescence properties of nano-sized $(Y_{0.5}Gd_{0.5})PO_4{:}Eu^{3+}$ phosphor powders synthesized by solution combustion method, Powder Technology 237 (2013) 102–106.
[15] S.R. Jain, K.C. Adiga, V.R. Pai Vernecker, A new approach to thermochemical calculations of condensed fuel-oxidizer mixtures, Combustion and Flame 40 (1981) 71–79.
[16] JCPDS file number 31-0022.
[17] K. Park, M.H. Heo, K.Y. Kim, S.J. Dhoble, Y. Kim, J.Y. Kim, Photoluminescence properties of nano-sized $(Y_{0.5}Gd_{0.5})PO_4{:}Eu^{3+}$ phosphor powders synthesized by solution combustion method, Powder Technology 237 (2013) 102–106.
[18] J.J. Kingsley, K. Suresh, K.C. Patil, Combustion synthesis of fine-particle metal aluminates, Journal of Materials Science 25 (1990) 1305–1312.
[19] M.T. Colomer, D.A. Fumo, J.R. Jurado, A.M. Segadaes, Non-stoichiometric $La_{(1-x)}NiO_{(3-\delta)}$ perovskites produced by combustion synthesis, Journal of Materials Chemistry 9 (1999) 2505–2510.
[20] R.-Y. Yang, H.-Y. Chen, S.-J. Chang, Y.-K. Yang, Effect of Eu^{3+} concentration on microstructure and photoluminescence of $Sr_2SiO_4{:}Eu^{3+}$

phosphors prepared by microwave, Journal of Luminescence 132 (2012) 780–783.
[21] Y. Liu, Z. Yang, A novel green luminescent material $AlPO_4:Tb^{3+}$, Materials Letters 65 (2011) 1853–1855.
[22] K. Park, M.H. Heo, S.J. Dhoble, VUV photoluminescence of green-emitting GdPO4:Tb,M (M: Al, Zn) synthesized by ultrasonic spray pyrolysis, Materials Chemistry Physics 140 (2013) 108–112.
[23] P. Li, L. Pang, Z. Wang, Z. Yang, Q. Guo, X. Li, Luminescent characteristics of $LiBaBO_3:Tb^{3+}$ green phosphor for white LED, Journal of Alloys and Compounds 478 (2009) 813–815.
[24] M. Weng, R. Yang, Y. Peng, J. Chen, Yellowish green-emitting $KSrPO_4:Tb^{3+}$ phosphors with various doping concentrations prepared by using microwave assisted sintering, Ceramics International 38 (2012) 1319–1323.
[25] Y. Fang, L. Li, Y. Chen, H. Wang, R. Zeng, Photoluminescence properties of Ce^{3+} and Ce^{3+}–Eu^{2+} energy transfer in $Ba_{1.3}Ca_{0.7}SiO_4$ phosphors, Journal of Luminescence 144 (2013) 13–17.
[26] J. Zhang, Y. Wang, Z. Zhang, Z. Wang, B. Liu, The relationship between photoluminescence quenching concentrations and excitation wavelengths in $(Gd,Y)BO_3$:Tb, Materials Letters 62 (2008) 202–205.
[27] G. Blasse, Energy transfer in oxidic phosphors, Physics Letters A 28 (1968) 444–445.
[28] D.L. Dexter, A theory of sensitized luminescence in solids, Journal of Chemical Physics 21 (1953) 836–850.
[29] D.L. Dexter, J.H. Schulman, Theory of concentration quenching in inorganic phosphors, Journal of Chemical Physics 22 (1954) 1063–1070.
[30] P.A.M. Berdowski, G. Blasse, Journal of Solid State Chemistry 63 (1986) 86–88.
[31] K. Toda, T. Honma, M. Sato, Unusual concentration quenching of europium luminescence in new layered perovskite compound, $RbLa_{1-x}Eu_xTa_2O_7$ $(0 \le x \le 1)$, Journal of Luminescence 71 (1997) 71–75.
[32] X. Zhang, X. Qiao, H.J. Seo, Red emission $LaMoBO_6:Eu^{3+}$ phosphor for near-UV white light-emitting diodes, Journal of the Electrochemical Society 157 (2010) J267–J269.
[33] D. Wang, Q. Yin, Y. Li, M. Wang, Concentration quenching of Eu^{2+} in $SrO \cdot Al_2O_3:Eu^{2+}$ phosphor, Journal of Luminescence 97 (2002) 1–6.
[34] L. Jiang, C. Chang, D. Mao, C. Feng, Concentration quenching of Eu^{2+} in $Ca_2MgSi_2O_7:Eu^{2+}$ phosphor, Materials Science and Engineering B 103 (2003) 271–275.
[35] S.S. Yao, L.H. Xue, Y.W. Yan, Concentration quenching of Eu^{2+} in $Ba_2Mg(BO_3)_2:Eu^{2+}$ phosphor, Current Applied Physics 11 (2011) 639–642.
[36] X. Zhang, H.J. Seo, Photoluminescence and concentration quenching of $NaCa_4(BO_3)_3:Eu^{3+}$ phosphor, Journal of Alloys and Compounds 503 (2010) L14–L17.
[37] L. Zhu, A. Lu, C. Zuo, W. Shen, Photoluminescence and energy transfer of Ce^{3+} and Tb^{3+} doped oxyfluoride aluminosilicate glasses, Journal of Alloys and Compounds 509 (2011) 7789–7793.